EVOLUTION OF OVERBURDEN FRACTURE AND WATER SEEPAGE IN COAL SEAM GROUP MINING
An Example in Lingxin Coal Mine

by

Qiang GUO[a,b], Jing-Feng LI[a*], Zhi-Guo CAO[a,b], and Jun-Ting GUO[a,b,c]

[a]China Energy Investment Group,
State Key Laboratory of Water Resource Protection and Utilization in Coal Mining, Beijing, China
[b]National Institute of Low Carbon and Clean Energy, Beijing, China
[c]School of Energy and Mining Engineering, China University of Mining and Technology, Beijing, China

Original scientific paper
https://doi.org/10.2298/TSCI2301671G

Taking Lingxin Coal Mine as the research object, the combination of physical experiment and numerical simulation analysis was used to study the mining failure of overlying strata and the development of surrounding rock cracks in goaf. The results show that when the underground coal seam mining is not sufficient, the overburden separation is developed, the connected pore area of the overburden failure accounts for about 20% of the total mining area. When the underground coal seam is fully mined, the overburden failure is severe, the overburden failure cracks are interconnected, and the connected pore area increases significantly.

Key words*: multi-seams, mining failure, overburden structure, fracture evolution, field of seepage*

Introduction

China has gradually shifted the focus of coal development to the western region with the gradual depletion of shallow buried coal resources in the eastern and central regions. However, there has a fragile ecological environment, and scarce water resources [1, 2]. The surface subsidence, groundwater pollution and other disasters caused by high-intensity coal mining activities are bound to seriously damage the ecological balance of the region and the security of the water resources system, causing incalculable impacts on the environment and people's production and life [3, 4].

Most of the mine water in coal areas in the western region is high salinity mine water If discharged to the natural environment directly, it will seriously affect the quality of surface water and further have different degrees of impact on land quality, agricultural production, and forest protection [5, 6]. Therefore, in order to reduce the impact of concentrated brine on the ecological environment and increase the efficiency of mine water, the technique of constructing underground reservoirs for concentrated brine storage which uses the goaf and protective coal pillars to form the closed space is proposed [7].

*Corresponding author, e-mail: 20024422@ceic.com

Due to the influence of mining, the equilibrium state of the original rock stress in the rock mass is destroyed, thus causing the redistribution of stress in the rock mass around the stopes, in front of the working face, the coal pillars and its roof and floor rock mass form a supporting pressure zone, and the goaf roof and floor rock mass form a reduced pressure zone [8, 9]. Therefore, using the goaf to construct underground reservoirs of the concentrated brine requires a study of overlying strata damage and fracture development in the surrounding rock of the goaf. To further illustrate the above viewpoint, a comparative simulation experimental study was carried out on the basis of actual measurements.

Analysis of overburden fracture distribution in coal seam group mining

The experiment is based on the fully mechanized mining face in the first mining area of Lingxin Coal Mine. The mining thickness of lower group 14#, 15# , and 16# coal seam is 2.78 m, 3.18 m, and 4.28 m, the dip angle is 10°, and the distance between 14#, 15#, and 16# coal seam is 20 m and 18 m, respectively. Each layer of coal mining has two working faces, a working face mining width of about 180 m, two working face interval coal pillar is about 25 m. The water source of the coal seam group roof is mainly the K2, K3, and K4 aquifer of the Yan'an group.

Table 1. Main mechanical properties parameters and layer thickness of rock

Rock stratum name	Compressive strength [MPa]	Tensile strength [MPa]	Volumetric weight [tm^{-3}]	Real thickness [m]	Cumulative true thickness [m]
Medium sandstone	37.2	2.5	2.66	9.5	279.9
Fine sandstone (K2)	40.6	2.8	2.68	43.2	270.4
Siltstone	43.4	3.5	2.66	47.8	227.2
Medium sandstone (K3)	37.2	2.5	2.66	8.4	179.4
Siltstone	43.4	3.5	2.66	84.1	171.1
Fine sandstone (K4)	40.6	2.8	2.68	17.8	87.0
Siltstone	43.4	3.5	2.66	18.4	69.2
14 coal	18.5	0.76	1.40	2.8	50.8
Siltstone	43.4	3.5	2.66	17.3	48.0
15 coal	18.5	0.76	1.40	3.2	30.7
Siltstone	43.4	3.5	2.66	11.3	27.6
16 coal	18.5	0.76	1.40	4.3	16.3
Mudstone	46	3.53	2.60	12.0	12.0

The plane similar material model was established by taking the inclined section of the first mining area of Lingxin Coal Mine. The size of the test model rack is 3.2 m (length) × 0.25 m (width) × 1.6 m (height). According to the similar simulation test bench size and mine geological data, the geometric similarity ratio C_j = 1:250, bulk density similarity ratio C_r = 1:1.5, and elastic modulus similarity ratio C_e = 1:375 of the model are determined. The cumulative height of the model design is 1.12 m (prototype 280 m). The thickness of the overlying strata that the model fails to simulate is 0.48 m (prototype 120 m), which should be realized by loading. The average bulk density of the strata in the model is 1666.7 kg/m^3. Therefore, the gravity compensation load that the model needs to apply is 2.67 kPa. The main mechanical property parameters and layer thickness of the working face are shown in tab. 1.

Analysis of similar simulation experiment

Overburden rock failure water inrush law of repeated mining in coal seam group

The mining of coal seam in the model is simulated according to the mining progress Working face mining sequence: L1614-L1616-L1816 fully mechanized working face. When mining L1614 working face of 14 coal seam, forming a trapezoidal failure zone. The trapezoidal top interface is 59 cm long, the normal height of failure is 8.6 cm, the failure angle of uphill is 65°, and the failure angle of downhill is 50°. The overburden failure zone is highly developed to the bottom of the K4 aquifer, and the fracture leads to the K4 aquifer, respectively, pouring three strands of water into the upper, middle, and lower edges of the working face. In the continuous mining of L1616 working face of 16 coal seam, the failure range of overlying strata is further expanded and developed upward. The overburden failure zone is highly developed into the K3 aquifer, and two water gushing points are added to the mountain edge of the L1616 working face. The continuous mining of 16 coal seam L1816 working face, the overburden rock failure zone is highly developed into the K3 aquifer, the downhill failure angle is 60°, the overburden rock is concave, and the cracking degree of the downhill crack connection is larger than that of the uphill direction. The asymmetric subsidence basin appears at the top of the model, step cracks appear in the downhill direction of the basin, the width is 6-10 mm, the drop is 2 mm, and there is no crack in the uphill direction. There is no water inflow in the mined-out area of the dip, and there are many water inflows in the mined-out area of the raise. After the end of mining and continuous water supply for a period of time, two water inflows appear above the L1816 mined-out area, but the water inflow is small.

Evolution law of displacement field of mining overburden rock

After the three working faces of L1614, L1616, and L1816 coal seams were mined in turn, the overlying strata produced movement and deformation. After taking photos and identifying the speckle measuring points collected, the overlying strata displacement field data was formed. The propagation direction of overburden displacement from bottom to top is vertical rather than normal. The displacement change diagram of overlying strata after mining of L1816 working face is shown in fig. 1. It can be seen that the overlying strata have collapsed, cracked, and separated after mining of L1816 working face. Because the isolated coal pillars of adjacent mining faces of 14 and 15 coal seams have been destroyed one after another, the failure range of overlying strata is further connected with the failure range of overlying strata in the L16 series goaf in the rise direction, and the failure range of overlying strata forms an overall failure zone. The displacement of overlying strata presents the characteristics of alarge basin as a whole. The subsidence of the same strata is centered on the whole goaf, with large subsidence in the middle and small subsidence on both sides.

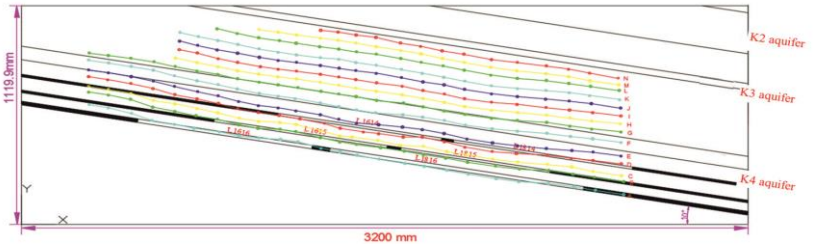

Figure 1. Overlying strata displacement change diagram

Evolution law of mining overburden fracture

In the similar simulation test, 3-D laser scanning was used to scan the development of the overburden fracture field, and the scanning results of the fracture field after mining in different working faces were compared and analysed. Figure 2 shows the identification results of model surface crack development after mining of L1614, L1616, and L1816 working faces. It can be seen that when the underground coal seam mining is not sufficient, the overburden strata separation development, the closed separation space area accounts for a large proportion, the goaf overburden strata connected pore space area accounts for a small proportion, and the overburden strata failure connected pore area accounts for about 20% of the total mining area When the underground coal seam is fully mined, the overburden failure is severe, the overburden failure cracks are interconnected, the connected pore area increases significantly, and the porosity can reach 70 %.

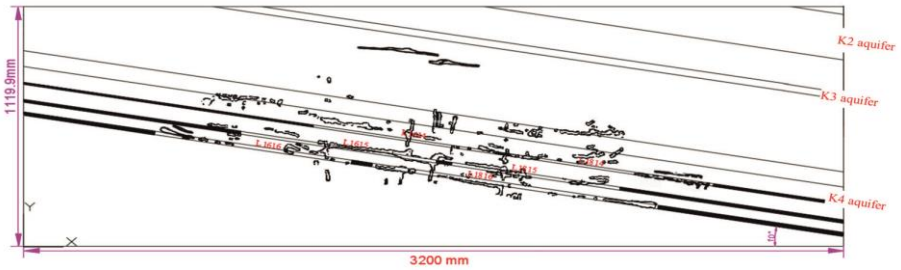

Figure 2. Recognition results of model surface crack development after mining

Evolution law of overburden seepage field in coal seam group mining

Numerical model building

Based on fig. 2, after the co-ordinate data of a single fracture node in the fracture network is obtained, the line unit of the fracture network is first established in GMSH software, and then the formation model is established. Finally, the 2-D plane model including the fracture network is established by Boolean operation. The triangular element is used and encrypted near the crack, where the crack is a one-dimensional line element. Finally, the numerical calculation model of the mining-induced fracture network was established, fig. 3.

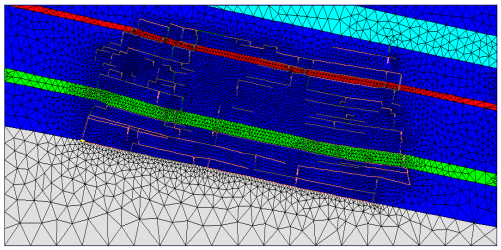

Figure 3. Numerical model

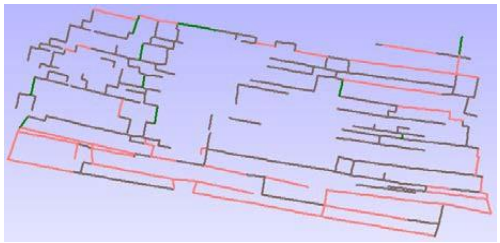

Figure 4. Diagram of crack classification

According to the crack opening, it is generally divided into three categories. As shown in fig. 4, the red crack is the crack with a large crack opening, the gray crack has the second largest crack opening, and the green crack has the smallest crack opening. The whole model is 1:1 scale of the prototype. Considering that the permeability of fine sandstone and siltstone is relatively small compared with the fracture, and this numerical simulation focuses

on the seepage in the fracture, fine sandstone and siltstone rock strata are unified as one material group in the numerical model. Therefore, the material groups in the model are divided into bottom mudstone, silty sand rock, aquifer K2, aquifer K3, aquifer K4, and three kinds of fractures. The unit size is 0.5 m minimum and 30 m maximum. The size of the fracture element is controlled within 1 m.

Seepage parameter setting

The OpenGeoSys numerical simulation platform is used for calculation. At present, the software is dedicated to solving the multi-physical field coupling problems of temperature, seepage, and stress in the fields of nuclear waste encapsulation, geothermal development, energy reserve, geological water resources, and geological water pollutant migration, *etc*., and has been applied in many fields involving the multi-physical field coupling problems of temperature, seepage, stress, and chemistry. The flow equation in the numerical calculation is given:

$$\frac{\partial(S\phi\rho)}{\partial t}+\nabla(\phi\rho\upsilon)=\rho Q \tag{1}$$

where υ is the flow rate and ρQ – the source/sink term of the aquifer. Here, eq. (1) is a special case considered in [10,11]. Thus, by eq. (1), we have:

$$\phi\frac{\partial S}{\partial t}+SS_0^h\frac{\partial h}{\partial t}+S\phi\lambda_C\frac{\partial C}{\partial t}+\nabla q+\lambda_C q\nabla C=Q \tag{2}$$

where S_0^h is the water storage coefficient and q – the Darcy's velocity. When pressure is used as a parameter, the relation between water head and water pressure is written as $h = p/(\rho g) + z$.

Considering the balance relation and calculating the concentration-based diffusion problem, west seepage in the case of unsteady concentration is suggested:

$$q=\phi\upsilon=-\frac{k\rho_0 g}{\mu}\left[\nabla h+\left(\frac{\rho-\rho_0}{\rho_0}\right)e\right] \tag{3}$$

where e is the gravity unit vector. The diffusion tensor of matter in liquid reads:

$$D=\gamma D_m\hat{\delta}+\alpha_T|\upsilon|\hat{\delta}+(\alpha_L-\alpha_T)\frac{\upsilon_i\upsilon_j}{|\upsilon|} \tag{4}$$

where γ is the pore curvature, D_m – the molecular diffusion coefficient, α_T – the transverse diffusion coefficient, α_L – the radial diffusion coefficient, and υ_i and υ_j are the flow rate in the direction of i and j, respectively. The solute transmission control azimuth reads:

$$\frac{\partial(\phi C)}{\partial t}+\nabla(\phi\upsilon C)-\nabla(\phi\hat{D}\nabla C)=Q_C \tag{5}$$

where Q_C is the source term of solute concentration. By synthesizing the required parameters in eqs. (1)-(5), the numerical simulation parameters used in this calculation are listed in tab. 2.

The permeability of cracks can be determined by:

$$k=\frac{b_h^2}{12} \tag{6}$$

where b_n is the diameter of the fracture. The average diameter of a large crack is 0.5 m, the average diameter of a medium crack is 0.2 m, and average diameter of a small crack is 0.01 m.

Table 2. Numerical simulation parameters of rock seepage

Unit of materials	Porosity [–]	Tortuosity [–]	Permeability [m^2]	Parameter of opening [–]
Mudstone	0.18	1	$1\cdot10^{-29}$	–
Silty sand rock	0.2	1	$1\cdot10^{-15}$	–
Aquifer K2	0.28	1	$2\cdot10^{-11}$	–
Aquifer K3	0.3	1	$1\cdot10^{-10}$	–
Aquifer K4	0.35	1	$1\cdot10^{-9}$	–
Large opening fracture	1	1	$2.08\cdot10^{-2}$	0.5
Medium opening fracture	1	1	$3.33\cdot10^{-3}$	0.2
Small opening fracture	1	1	$8.33\cdot10^{-6}$	0.01

Seepage law of fissure under water injection condition

One year after water injection, as shown in fig. 5(a), the concentrated brine is mainly in the cracks, and some concentration is distributed in the broken rock in the fault zone. Within 5-10 years, as shown in fig. 5 (b), the concentrated brine in the fracture gradually diffuses to the rock mass. The concentrated brine in the fracture of L1614 uphill diffuses rapidly, mainly because the concentrated brine goes deep into the fracture and diffuses along the fracture water under the action of the concentration gradient. In 50 years, the concentrated brine is mainly concentrated in the K4 aquifer and the fractured rock below it. In 50 years, due to the existence of the concentration gradient, the concentrated brine in the K4 aquifer will slowly diffuse upward. But after 10 years, the diffusion of the salt water slowed significantly due to its own gravity. After 40 years, the K3 aquifer had only a slight saline concentration distribution, concentrated brine concentration of about 0.1-0.3, indicating that the concentrated brine barely diffused to the K3 aquifer.

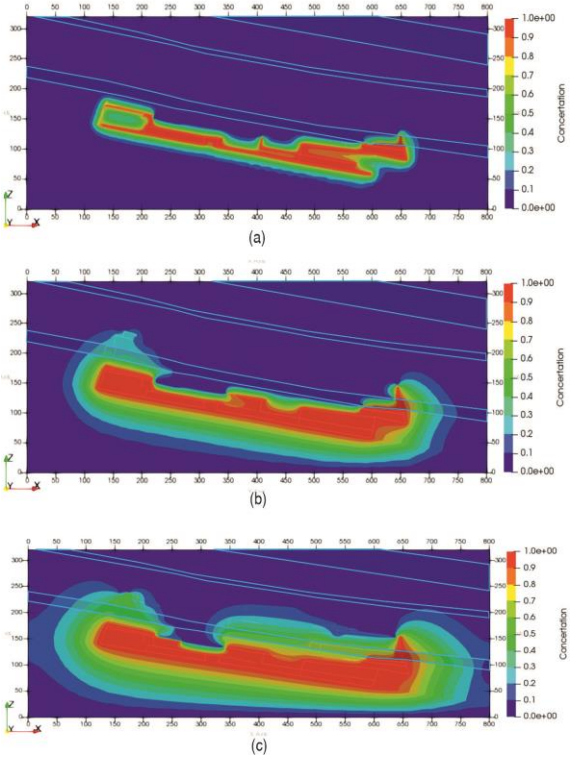

Figure 5. Evolution of concentration field after water injection; (a) t = 1 year, (b) t = 10 year, and (c) t = 30 year

Conclusion

Taking the coal seam group mining of Lingxin Coal Mine as the research object, the evolution law of overlying fracture field and seepage field in coal seam group mining was systematically studied. The overburden fractures caused by repeated mining in the working face are mainly distributed in the rock strata adjacent to the goaf, in the form of bed separation fractures and partial fracture fractures. The near-surface fractures are mainly separation fractures and extend to K3 aquifer. The floor and surrounding rock of the goaf have good water isolation.

Nomenclature

D – Diffusion tensor, [m^2s^{-1}]
k – permeability, [m^2]
q – Darcy's velocity,[ms^{-1}]
t – time, [s]

Greek symbols

$\hat{\delta}$ – Kronecker symbol, [s]
ρ – density, [kgm^{-3}]
ϕ – porosity, [%]

References

[1] Bian, W., *et al.*, Design of Sodium Hypochlorite Disinfection System in Huyan Water Treatment Plant, *Technology of Water Treatment*, *47* (2021), Aug., pp. 1-7
[2] Lei, S., *et al.*, Research Progress on the Environment Impacts from Underground Coal Mining in Arid Western Area of China, *Acta Ecologica Sinica*, *34* (2014), Jan., pp. 2837-2843
[3] Chen, S., *et al.*, Technology of Underground Reservoir Construction and Water Resource Utilization in Daliuta Coal Mine, *Coal Science and Technology*, *44* (2016), Aug., pp. 21-28
[4] Gu, D., *et al.*, Technical Progress of Water Resource Protection and Utilization by Coal Mining in China, *Coal Science and Technology*, *44* (2016), Jan., pp. 1-7
[5] Guo, Q., *et al.*, Treatment of High Salinity Mine Water and Storage of Concentrated Brine, *Coal Engineering*, *52* (2022), Dec., pp. 16-19
[6] Qian, M., *et al.*, Green Mining of Coal Resources Harmonizing with Environment, *Journal of China Coal Society*, *32* (2007), Jan., pp. 1-7
[7] Gu, D., Theory Framework and Technological System of Coal Mine Underground Reservoir, *Journal of China Coal Society*, *40* (2015), Feb., pp, 239-246
[8] Kang, Y., *et al.*, The Damage Law of the Overlying Strata of the Repeated Mining in Combined Mining, *Coal Science and Technology*, *29* (2001), Jan., pp. 22-24
[9] Li, H., *et al.*, Experimental Study on Characteristics of Groundwater Fracture in Coal Mine Overlying Rock, *Coal Science and Technology*, (2022), May., pp. 1-10
[10] Yang, X. J., An Insight on the Fractal Power Law Flow: From a Hausdorff Vector Calculus Perspective, *Fractals*, *30* (2022), 3, pp. 2250054-929
[11] Yang, X. J., *et al.*, A New Insight to the Scaling-law Fluid Associated with the Mandelbrot Scaling Law, *Thermal Science*, *25* (2021), 6B, pp.4561-4568

Paper submitted: August 21, 2022
Paper revised: November 15, 2022
Paper accepted: November 22, 2022
© 2023 Society of Thermal Engineers of Serbia.
Published by the Vinča Institute of Nuclear Sciences, Belgrade, Serbia.
This is an open access article distributed under the CC BY-NC-ND 4.0 terms and conditions.